Electronic Supplementary Material (ESI) for Materials Advances.
This journal is © The Royal Society of Chemistry 2021

Supporting information

Doped and non-doped blue organic light-emitting diodes based on AIEgens with high exciton utilization efficiency and external quantum efficiency

Jayaraman Jayabharathi*, Sekar Sivaraj, Venugopal Thanikachalam, Jagathratchagan Anudeebhana

Department of Chemistry, Material Science Lab, Annamalai University, Annamalai Nagar, Tamilnadu- 608 002, India

Contents

SI-I. (i) General information

All the reagents and solvents were purchased from commercial sources and used as received. The emitters were subjected to sublimation to enhance the purity before photoluminescence and electroluminescence investigations. ^{1}H and ^{13}C NMR spectra were recorded at room temperature on Bruker 400 spectrometer in CD_2Cl_2. The mass spectra were recorded on Agilent LCMS VL SD. The UV-Vis spectra were recorded on Lambda 35 PerkinElmer (solution)/ Lambda 35 spectrophotometer (RSA-PE-20) (film). The emission spectra were recorded with Perkin Elmer LS55 spectrometer and quantum yield was measured with fluorescence spectrometer (Model-F7100 with integrating sphere). The decomposition temperature (T_d) and glass transition temperature (T_g) were measured with Perkin Elmer thermal analysis system (10° C min^{-1}; N_2 flow rate - 100 ml min^{-1}) and NETZSCH (DSC-204) (10° C min^{-1}; N_2 atmosphere), respectively. Fluorescence lifetime was estimated by time correlated single-photon counting (TCSPC) method on Horiba Fluorocube-01-NL lifetime system: nano LED is an excitation source with TBX-PS is detector; DAS6 software was employed to analyze the decay by reconvolution method. Oxidation potential of these materials was measured from potentiostat electrochemical analyzer (CHI 630A) in dichloromethane at a scan rate of 100 mV s^{-1}, using a platinum wire as auxiliary electrode, a glass carbon disk as working electrode and Ag/Ag^{+} as reference electrode. Ferrocene was used as an internal standard with HOMO of -4.80 eV and 0.1M tetrabutylammonium perchlorate in CH_2Cl_2 as supporting electrolyte. All density functional theory (DFT) calculations were carried out using Gaussian 09 package [1] and Multiwfn [1]. The ground-state (S0) geometries in the gas phase were initially optimized at the level of B3LYP/6-31G (d, p), a commonly used level for the precise geometry optimization. Then, geometry optimization of S1 and excited-state properties based on S1 geometries were studied using time-dependent DFT (TD-DFT) at the same level. The natural transition orbitals (HONTOs & LUNTOs) with hole-particle contribution,

transition density matrix and overlap integral were studied in detail.

(ii) OLEDs fabrication and measurement

ITO glass (resistance 20 Ω/sq) were cleaned with acetone, deionized water and isopropanol and dried (120 ^{o}C) followed by UV-zone treatment (20 min) and transferred into deposition system. The devices were fabricated by multiple source beam deposition method (vacuum pressure -4 × 10^{-5} mbar). Evaporation rate of 2-4 Å s^{-1} (organic materials) and 0.1 and 4 Å s^{-1} for LiF and metal electrodes were applied, respectively. The thickness of each decomposition layer was monitored with quartz crystal thickness monitor. The EL measurement was recorded with USB-650-VIS-NIR spectrometer (Ocean Optics, Inc, USA). The current density-voltage-luminance (J-V-L) characteristics was performed using source meter (Keithley 2450) equipped with LS-110 light intensity meter. The external quantum efficiency was determined from luminance, current density and EL spectrum assuming Lambertian distribution.

(iii) Synthesis of emissive materials

Synthetic route of the emissive materials has been outlined in Scheme S1.

(a) (*E*)-5,10-dibromo-1-(naphthalen-1-yl)-2-styryl-1H-phenanthro[9,10-d]imidazole (DBSPI)

A mixture of 2,7-dibromophenanthrene-9,10-dione (2 mmol), cinnamaldehyde (2 mmol), naphthalen-1-amine (10 mmol) and ammonium acetate (8 mmol) in acetic acid (20 mL) was refluxed with continuous stirring for 24 h (120°C; N_2) and then poured into methanol. The resulting solid was filtered, washed with water and dried. The intermediate DBSPI was collected as pale yellow solid. Yield: 75%. ^{1}H NMR (400 MHz; $CDCl_3$; δ, ppm): 6.92 (d, 2H), 7.14-7.21 (m, 3H), 7.30-7.38 (m, 6H), 7.70 (t, 3H), 8.06 (d, 2H), 8.29 (S, 2H), 8.82 (d, 2H). ^{13}C NMR (100 MHz; $CDCl_3$; δ, ppm): 112.8, 120.9, 126.3, 124.1, 125.3, 126.4, 127.2, 128.0, 129.8, 130.5, 131.6, 133.4, 134.6, 135.2, 141.5.

(b) (E)-4-(5,10-dibromo-2-styryl-1H-phenanthro[9,10-d]imidazol-1-yl)-1-naphthonitrile (DBSPI-NCN)

The similar procedure was followed as that described for DBSPI instead of naphthalen-1-amine, 4-amino-1-naphthonitrile was used. The intermediate DBSPI-NCN was collected as pale yellow solid. Yield: 65%. ^{1}H NMR (400 MHz; $CDCl_3$; δ, ppm): 6.90 (d, 2H), 7.10-7.30 (m, 5H), 7.74-7.80 (m, 5H), 8.05-8.20 (t, 3H), 8.28 (s, 2H), 8.71 (d, 2H). ^{13}C NMR (100 MHz; $CDCl_3$; δ, ppm): 109.5, 112.8, 115.8, 120.9, 121.7, 123.8, 124.6, 126.5, 127.5, 128.0, 128.7, 129.8, 130.5, 131.6, 132.7, 133.4, 136.0, 141.5.

(c) 1-(naphthalen-1-yl)-5,10-bis(4-(2,2-diphenylvinyl)phenyl)-2-styryl-1H-phenanthro [9,10-d]imidazole (NSPI-DVP)

A mixture of DBSPI (2mmol), (4-(2,2-diphenylvinyl)phenyl)boronic acid (6 mmol), $Pd(PPh_3)_4$ (0.4mmol) and K_2CO_3 (6 mmol) was refluxed in a mixture of solvents (toluene, ethanol and water (8:1:1)) for 24 h in nitrogen stream. The reaction mixture was extracted with dichloromethane and the residue was purified by column chromatography. The NSPI-DVP was separated as white powder. Yield: 65%. ^{1}H NMR (400 MHz, $CDCl_3$, δ, ppm): 6.78 (s, 2H), 6.89 (d, 2H), 7.11-7.21 (m, 7H), 7.24-7.26 (m, 8H), 7.36-7.42 (m, 10H), 7.48-7.63 (m, 11H), 7.70 (t, 3H), 8.10-8.34 (m, 5H), 8.99 (d, 2H). ^{13}C NMR (100 MHz, $CDCl_3$, δ, ppm): 112.8, 122.9, 124.0, 125.2, 126.0, 126.6, 127.8, 128.0, 130.4, 132.2, 133.4, 134.1, 135.7, 137.7, 140.0, 141.5. Anal. Calcd (%) for $C_{73}H_{50}N_2$: C, 91.79; H, 5.28; N, 2.93. Found: C, 91.76; H, 5.26; N, 2.90. MS: m/z. 955.00 [M^+]; Calcd. 955.02.

(d) (E)-4-(5,10-bis(4-(2,2-diphenylvinyl)phenyl)-2-styryl-1H-phenanthro[9,10-d]imidazol-1-yl)-1-naphthonitrile (CNSPI-DVP)

The synthetic procedure was similar to that described for NSPI-DVP instead of DBSPI, DBSPI-NCN was used. Yield: 60%. ^{1}H NMR (400 MHz; $CDCl_3$; δ, ppm): 6.60 (d, 2H), 6.89 (d, 2H), 7.05-7.20 (m, 7H), 7.30-7.35 (m, 10H), 7.40-7.42 (m, 9H), 7.50-7.58 (m, 9H), 7.60-7.80 (t, 3H), 8.12 (d, 2H), 8.20 (s, 1H), 8.38 (d, 2H), 8.80 (d, 2H). ^{13}C NMR (100 MHz; $CDCl_3$; δ, ppm): 109.5, 112.8, 115.8, 121.7, 122.9, 123.8, 124.0, 125.2, 126.0, 126.6, 127.5, 127.8,

128.0, 128.7, 130.4, 132.7, 133.4, 134.1, 135.2, 137.3, 140.0, 141.5. Anal. Calcd (%) for $C_{74}H_{49}N_3$: C, 90.67; H, 5.04; N, 4.29. Found: C, 90.66; H, 5.02; N, 4.26. MS: m/z. 980.08 [M^+]; Calcd. 980.10.

Scheme S1. Synthetic route of emissive materials.

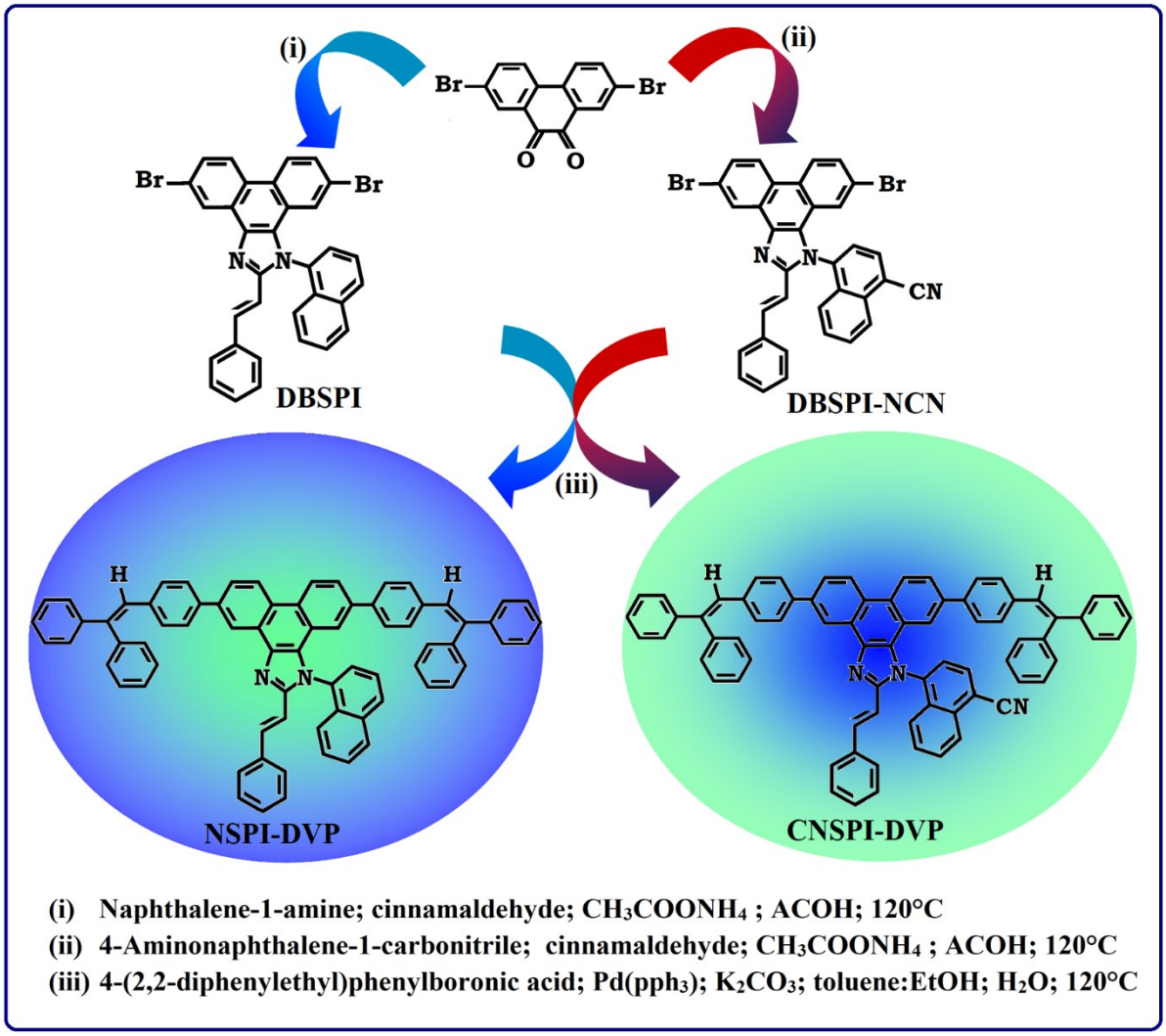

SI–II: Charge–Transfer intexes

The hole–particle pair interactions have been related to the distance covered during the excitations one possible descriptor Δr intex could be used to calculate the average distance which is weighted in function of the excitation coefficients.

$$\Delta r = \frac{\Sigma_{ia} k_{ia}^2 \left| \langle \varphi_a | r | \varphi_a \rangle - \langle \varphi_i | r | \varphi_i \rangle \right|}{\Sigma_{ia} K_{ia}^2} \quad \text{…….. (S1)}$$

where $\left| \langle \varphi_i | r | \varphi_i \rangle \right|$ is the norm of the orbital centroid [2–5]. Δr–index will be expressed in Å. The density variation associated to the electronic transition is given by

$$\Delta\rho(r) = \rho_{EX}(r) - \rho_{GS}(r) \quad \text{..... (S2)}$$

where $\rho_{GS}(r)$ and $\rho_{EX}(r)$ are the electronic densities of to the ground and excited states, respectively. Two functions, $\rho_+(r)$ and $\rho_-(r)$, corresponds to the points in space where an increment or a depletion of the density upon absorption is produced and they can be defined as follows:

$$\rho_+(r) = \begin{Bmatrix} \Delta\rho(r) & if\ \Delta\rho(r) > 0 \\ 0 & if\ \Delta\rho(r) < 0 \end{Bmatrix} \quad \text{..... (S3)}$$

$$\rho_-(r) = \begin{Bmatrix} \Delta\rho(r) & if\ \Delta\rho(r) < 0 \\ 0 & if\ \Delta\rho(r) > 0 \end{Bmatrix} \quad \text{..... (S4)}$$

The barycenters of the spatial regions R_+ and R_- are related with $\rho_+(r)$ and $\rho_-(r)$ and are shown as

$$R_+ = \frac{\int r\rho_+(r)dr}{\int \rho_+(r)dr} = (x_+, y_+, z_+) \quad \text{..... (S5)}$$

$$R_- = \frac{\int r\rho_-(r)dr}{\int \rho_-(r)dr} = (x_-, y_-, z_-) \quad \text{..... (S6)}$$

The spatial distance (D_{CT}) between the two barycenters R_+ and R_- of density distributions can thus be used to measure the CT excitation length

$$D_{CT} = \left| R_+ - R_- \right| \quad \text{(S7)}$$

The transferred charge (q_{CT}) can be obtained by integrating over all space $\rho_+ (\rho_-)$,. Variation in dipole moment between the ground and the excited states (μ_{CT}) can be computed by the following relation:

$$\|\mu_{CT}\| = D_{CT} \int \rho_+ (r) dr = D_{CT} \int \rho_- (r) dr \quad \text{(S8)}$$

$$= D_{CT} q_{CT} \quad \text{(S9)}$$

The difference between the dipole moments $\|\mu_{CT}\|$ have been computed for the ground and the excited states $\Delta\mu_{ES-GS}$. The two centroids of charges (C^+/C^-) associated to the positive and negative density regions are calculated as follows. First the root–mean–square deviations along the three axis (σ_{aj}, j = x, y, z; a = + or –) are computed as

$$\sigma_{a,j} = \sqrt{\frac{\sum_i \rho_a(r_i)(j_i - j_a)^2}{\sum_i \rho_a (r_i)}} \quad \text{(S10)}$$

The two centroids (C_+ and C_-) are defined as

$$C_+ (r) = A_+ \, e \left(-\frac{(x - x_+)^2}{2\sigma_{+x}^2} - \frac{(y - y_+)^2}{2\sigma_{+y}^2} - \frac{(z - z_+)^2}{2\sigma_{+z}^2} \right) \quad \text{(S11)}$$

$$C_- (r) = A_- \, e \left(-\frac{(x - x_-)^2}{2\sigma_{-x}^2} - \frac{(y - y_-)^2}{2\sigma_{-y}^2} - \frac{(z - z_-)^2}{2\sigma_{-z}^2} \right) \quad \text{(S12)}$$

The normalization factors (A+ and A_) are used to impose the integrated charge on the centroid to be equal to the corresponding density change integrated in the whole space:

$$A_{+} = \frac{\int \rho_{+}(r)dr}{\int e(-\frac{(x-x_{-})^2}{2\sigma_{+x}^2} - \frac{(y-y_{-})^2}{2\sigma_{+y}^2} - \frac{(z-z_{-})^2}{2\sigma_{+z}^2})dr} \quad \text{..... (S13)}$$

$$A_{-} = \frac{\int \rho_{-}(r)dr}{\int e(-\frac{(x-x_{-})^2}{2\sigma_{-x}^2} - \frac{(y-y_{-})^2}{2\sigma_{-y}^2} - \frac{(z-z_{-})^2}{2\sigma_{-z}^2})dr} \quad \text{..... (S14)}$$

H index is defined as half of the sum of the centroids axis along the D–A direction, if the D–A direction is along the X axis, H is defined by the relation:

$$H = \frac{\sigma_{+x} + \sigma_{-x}}{2} \quad \text{..... (S15)}$$

The centroid along X axis is expected. The t intex represents the difference between D_{CT} and H:

$$t = D_{CT} - H \quad \text{..... (S16)}$$

The interstate hybridization coupling between LE and CT state wave function are of $\Psi_{S_1/S_2} = c_{LE}.\Psi_{LE} \pm c_{CT}.\Psi_{CT}$. The % CT of these emitters increases as increasing the aromatic fragment size and also partially influenced by steric hindrance. The % LE in S_1 state, these emitters exhibit higher photoluminance efficiency (η_{PL}) and high lying CT state increased the EUE (Figure12). Therefore, degree of hybridization between LE and CT states depends not only initial E_{LE}-E_{CT} energy gap but also their interstate coupling strength [6]. The existence LE and CT states can be discussed from wave function of electron-hole pairs transition density matrix (TDM) plot. The diagonal region represents LE component and off-diagonal region shows CT component. Upon excitation, electron is transferred from donor and localized on acceptor: depending upon intramolecular geometrical and electronic coupling, transferred electron is delocalized from the region of nearby donor to the vicinity of acceptor. This effect can be qualitatively studied by analyzing electron density distribution at ground and excited

states. Computed electron-hole properties, distance between hole and electron, transition density, H and t indexes and RMSD of electron and hole of these emitters are displayed in Tables S7 and S8.

The integral value of hole and electron with transition density is shown in Tables S5&S6. The integral overlap of hole-electron distribution (S) is a measure of spatial separation of hole and electron. The integral overlap (S) of hole and electron and distance (D) between centroids of hole and electron proved the existence of LE and CT states. These emitters show small S and high D, indicates higher charge transfer (CT) variation of dipolemoment with respect to S_0 state. These values are directly evaluated based on the position of centroid of hole and electron. RMSD of hole or electron characterizes their distribution breadth: RMSD of both electron and hole is higher in X direction indicates electron and hole distribution is much broader in Y and Z directions (Tables S7&S8). The overlap between the region of density depletion and increment have been visualised by using two centroids of charges (equations S9 and S10). The H and t indexes for NSPI-DVP and CNSPI-DVP are tabulated (Tables S5 & S6). The CT intex, *i.e.* index difference between D_{CT} and H index is another measure of the separation of hole-electron (equations S15 and S16). The D_{CT}/μ_{CT} of NSPI-DVP and CNSPI-DVP has been calculated to be 0.99/ 0.001 and 0.18 /602.41, respectively and H/t indexes of NSPI-DVP and CNSPI-DVP has calculated to be 8.49/7.97 and 2.57/3.46, respectively (6).

The hybridization of these materials have been further evidenced by Δr intex (Tables S1&S2). The Δr intex (equation S1) is average of hole (h^+)-electron (e^-) distance ($d_{h^+ - e^-}$) upon excitation which indicates the nature of excitation type, LE or CT: valence excitation (LE) is related to short distances ($d_{h^+ - e^-}$) while larger distances ($d_{h^+ - e^-}$) related to CT excitation. The triplet exciton is transformed to singlet exciton *via* RISC process with high energy excited state (hot CT channel) [7, 8] which are beneficial for triplet exciton conversion in electroluminescence process without delayed fluorescence. The CT excitons have been formed

with weak binding energy (E_b) on higher excited states [9, 10]. As a result, the exciton utilization can be harvested in NSPI-DVP and CNSPI-DVP like phosphorescent materials. The hybridization between LE and CT components leads to high EUE and enhanced OLEDs performances (Table 3) [10].

SI–II: Figures

Figure S1. Natural transition orbital pairs (HONTOs and LUNTOs) with transition character of CNSPI-DVP [*f*-oscillator strength and % weights of hole-particle].

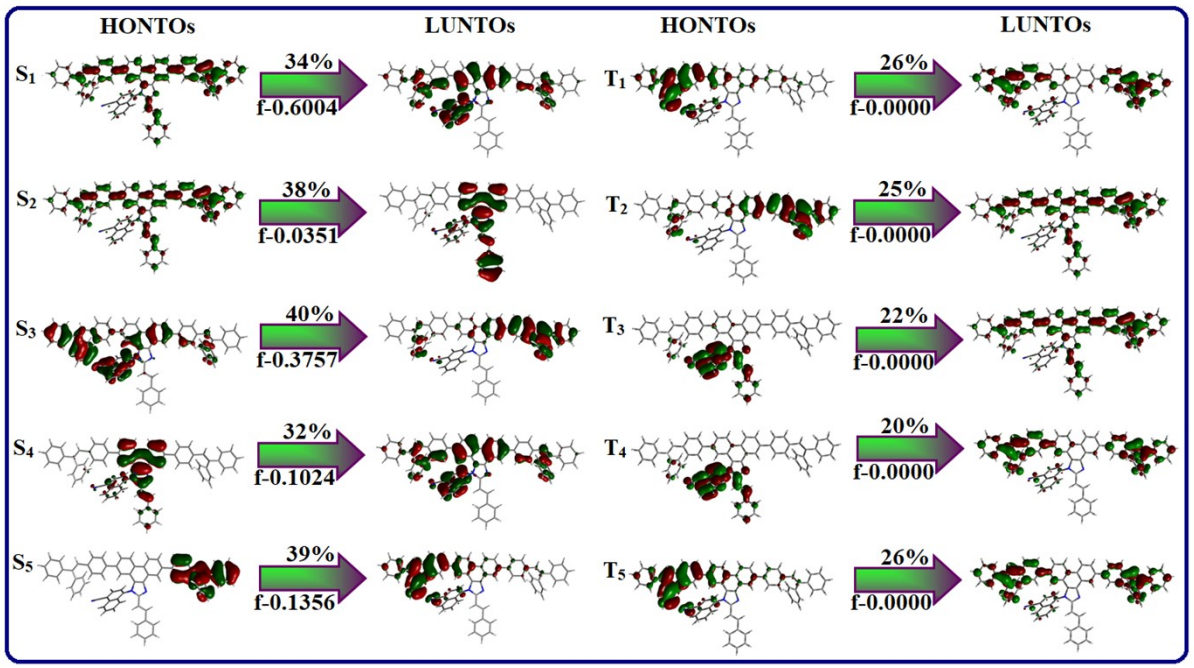

Figure S2. Solvatochromism: Absorption and Emission spectra of NSPI-DVP (a, b) and CNSPI-DVP (c, d).

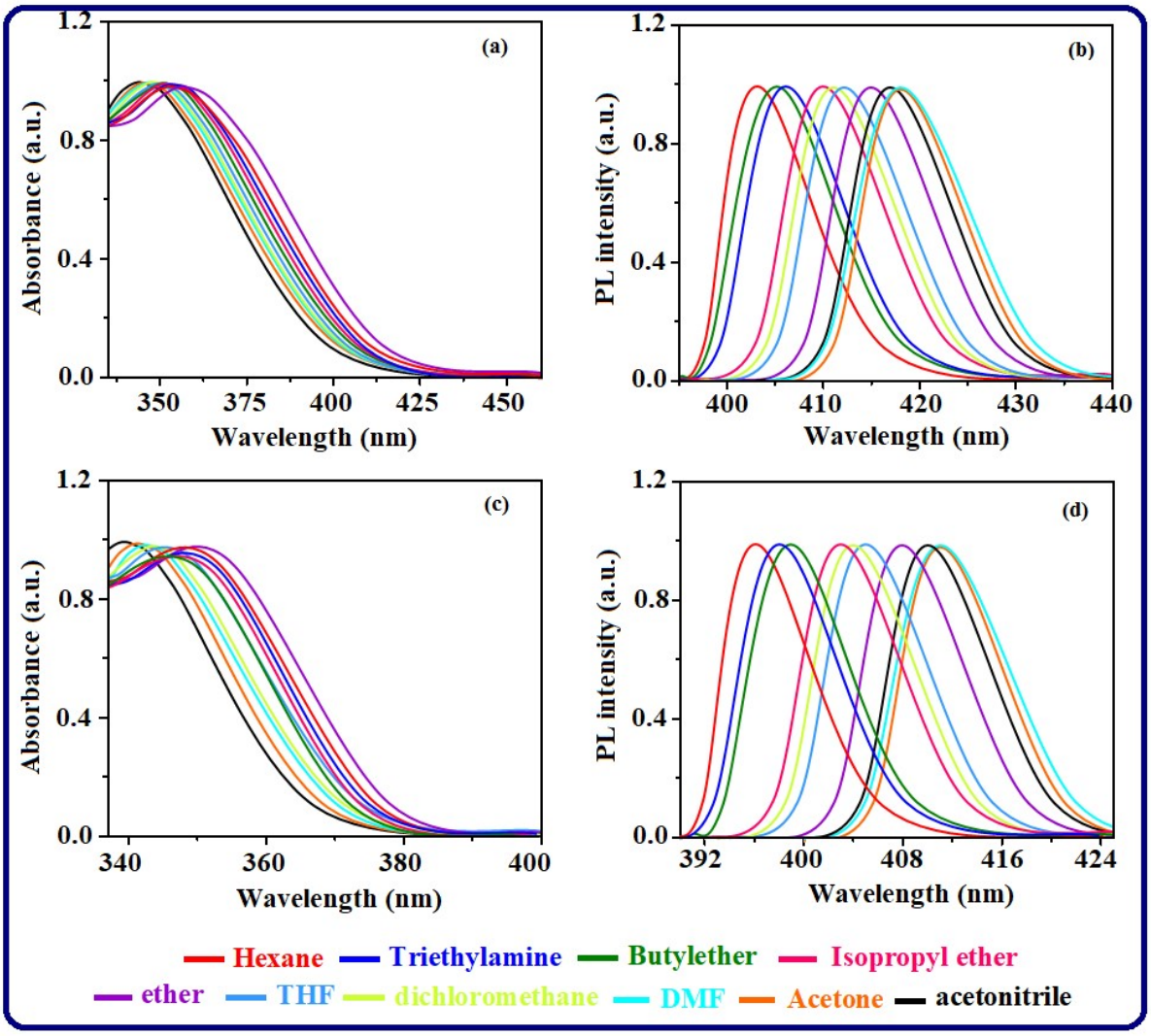

Figure S3. (a) Schematic representation of RISC process by high-lying CT states and (b) Hybridization process of LE and CT states of NSPI-DVP.

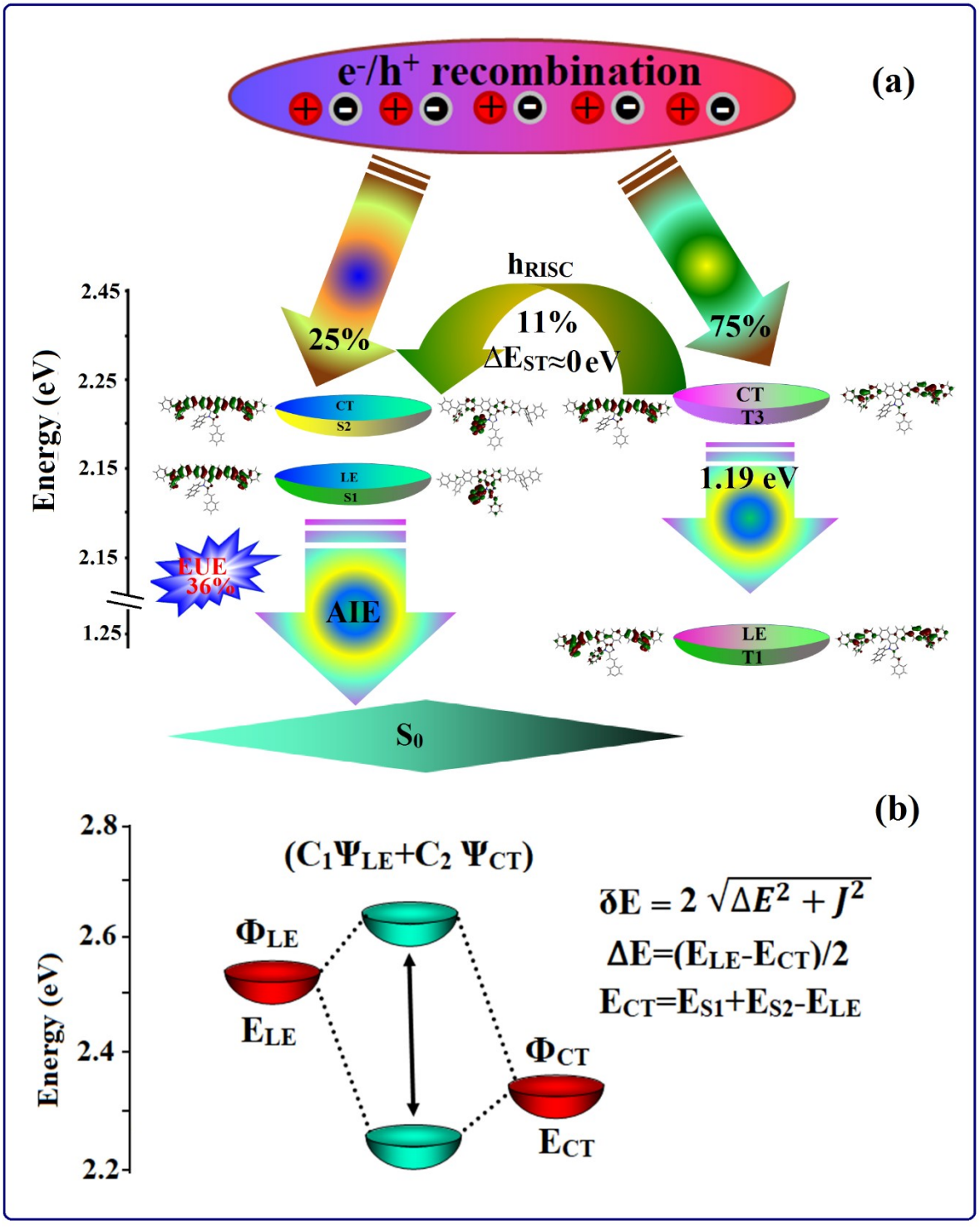

Figure S4. Hole and particle distribution green - increasing electron density and blue - decreasing electron density and Contour plots of transition density matrices (TDM) of NSPI for [S_1-S_4 states: density=transition=n /IOp(6/8=3)].

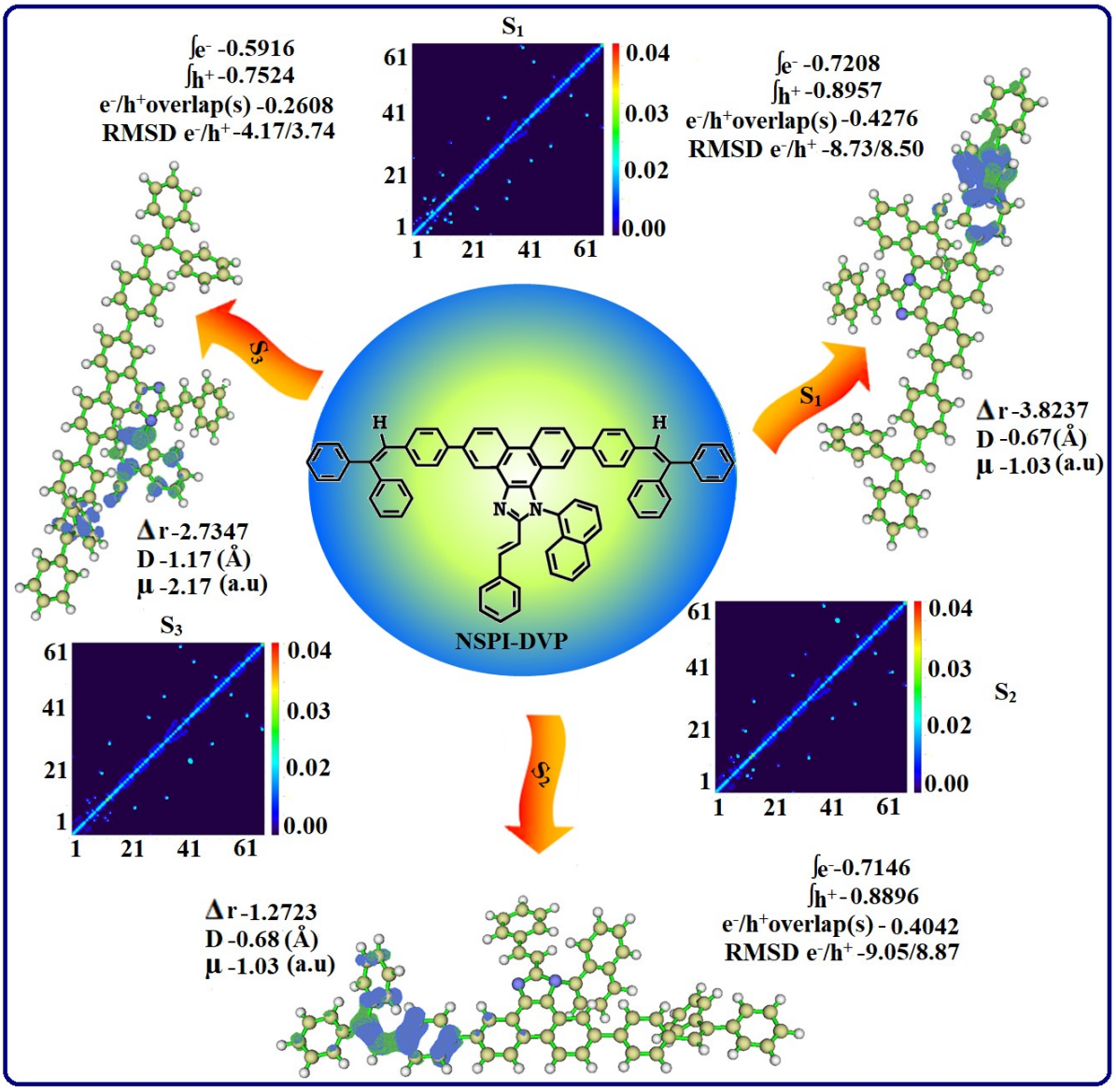

Figure S5. Energy level diagram of (a) Non- doped and (b) Doped devices and (c) Current density-electric field intensity curves of single carrier devices based on NSPI-DVP and CNSPI-DVP.

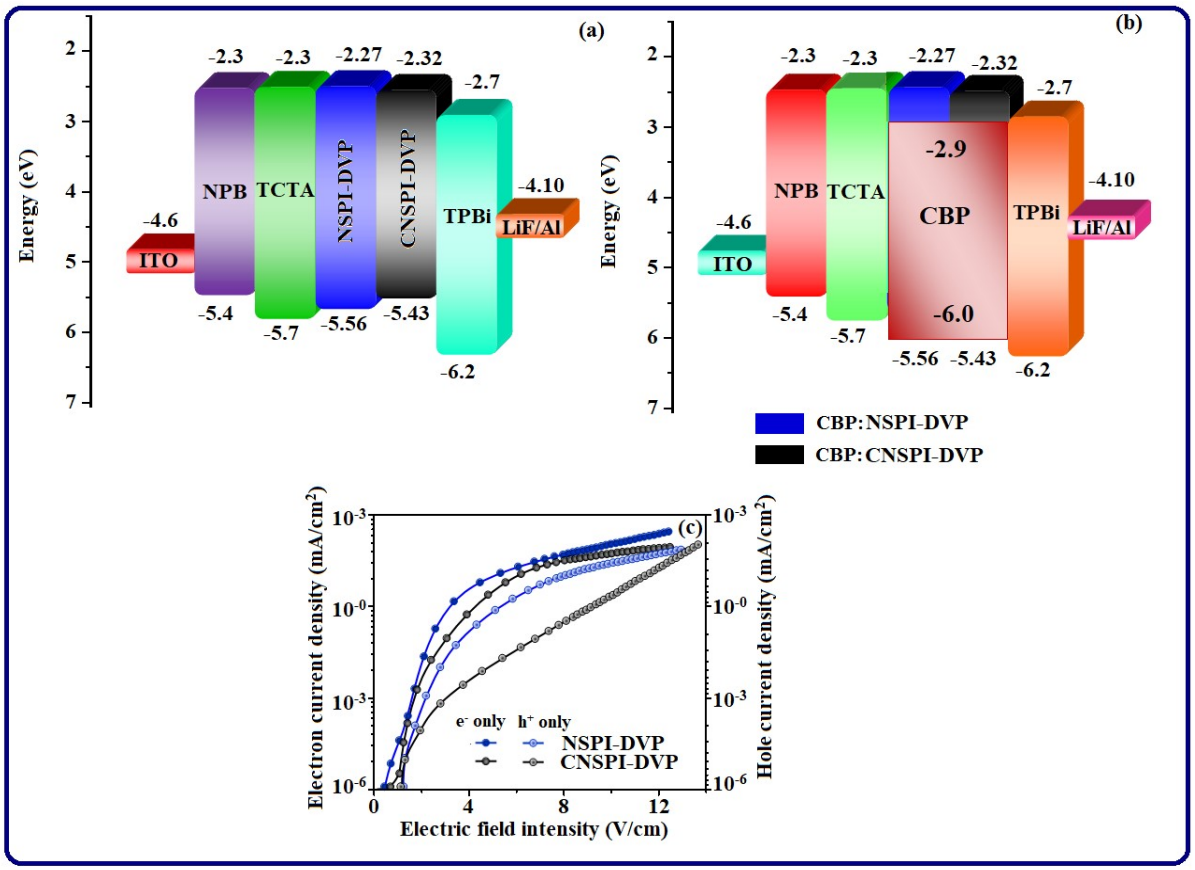

SI–III: Tables

Table S1: Computed excitation energy (EV), excitation coefficient, Δr intex (Å) Oscillator strength and dipolemoment (μ) for singlet and triplet states of NSPI-DVP.

State	Excitation energy	Excitation coefficient	Δr intex	Oscillator strength (f)	μ	NTO Transitions
S1	2.15	0.4393	3.8237	0.1511	1.03	$180 \xrightarrow{38\%} 184$
S2	2.23	0.4363	1.2723	0.4867	1.03	$179 \xrightarrow{42\%} 183$
S3	2.70	0.3676	2.7347	0.5285	2.17	$180 \xrightarrow{26\%} 181$
S4	2.73	0.3605	2.3984	0.5776	0.99	$178 \xrightarrow{44\%} 182$
S5	3.33	0.3965	1.7759	0.0936	0.44	$178 \xrightarrow{21\%} 183$
T1	1.28	0.2788	4.1409	0.0000	0.98	$174 \xrightarrow{19\%} 178$
T2	1.54	0.2935	2.2175	0.0000	0.88	$176 \xrightarrow{22\%} 178$
T3	2.22	0.3711	1.1685	0.0000	0.39	$173 \xrightarrow{46\%} 180$
T4	2.30	0.2690	2.8919	0.0000	0.68	$174 \xrightarrow{19\%} 178$
T5	2.66	0.1331	4.3415	0.0000	0.36	$176 \xrightarrow{22\%} 178$

Table S2: Computed excitation energy (EV), excitation coefficient, Δr intex (Å) Oscillator strength and dipolemoment (μ) for singlet and triplet states of CNSPI-DVP.

State	Excitation energy	Excitation coefficient	Δr intex	Oscillator strength (f)	μ	NTO Transitions
S1	2.48	0.4091	7.1934	0.6004	0.67	$174 \xrightarrow{34\%} 178$
S2	2.88	0.4017	5.9761	0.0351	0.62	$176 \xrightarrow{38\%} 178$
S3	3.30	0.3899	4.3923	0.3757	1.20	$175 \xrightarrow{40\%} 179$
S4	3.34	0.3511	2.8211	0.1024	2.40	$176 \xrightarrow{32\%} 177$
S5	3.39	0.3602	3.1305	0.1356	0.55	$173 \xrightarrow{39\%} 180$
T1	2.34	0.2640	6.9139	0.0000	1.38	$180 \xrightarrow{26\%} 184$
T2	2.57	0.2539	6.0156	0.0000	1.40	$179 \xrightarrow{25\%} 183$
T3	2.62	0.3133	3.0661	0.0000	0.57	$176 \xrightarrow{22\%} 181$
T4	2.78	0.3033	3.2633	0.0000	0.21	$176 \xrightarrow{20\%} 184$
T5	2.87	0.1803	3.1806	0.0000	0.36	$180 \xrightarrow{26\%} 184$

Table S3: Photophysical properties of NSPI-DVP in different solvents.

Solvents	**ε**	**n**	**f (ε,n)**	**λ_{ab} (nm)**	**υ_{ab} (cm^{-1})**	**λ_{flu} (nm)**	**υ_{flu} (cm^{-1})**	**υ_{ss} (cm^{-1})**
Hexane	1.88	1.37	0.0004	353	28329	403	24814	3515
Triethylamine	2.42	1.40	0.048	353	28329	406	24631	3698
Butylether	3.08	1.39	0.096	351	28490	405	24691	3799
Isopropyl ether	3.88	1.37	0.145	352	28409	410	24390	4019
ether	4.27	1.35	0.165	355	28169	415	24096	4077
THF	7.52	1.40	0.209	350	28571	412	24272	4300
dichloromethane	9.08	1.42	0.218	348	28736	411	24331	4405
DMF	36.7	1.43	0.276	347	28818	418	23923	4895
Acetone	21.01	1.36	0.285	346	28902	418	23923	4978
acetonitrile	37.5	1.34	0.305	344	290707	417	23981	5089

Table S4: Photophysical properties of CNSPI-DVP in different solvents.

Solvents	**ε**	**n**	**f (ε,n)**	**λ_{ab} (nm)**	**υ_{ab} (cm^{-1})**	**λ_{flu} (nm)**	**υ_{flu} (cm^{-1})**	**υ_{ss} (cm^{-1})**
Hexane	1.88	1.37	0.0004	348	28736	396	25253	3483
Triethylamine	2.42	1.40	0.048	348	28736	399	25063	3673
Butylether	3.08	1.39	0.096	346	28902	398	25126	3776
Isopropyl ether	3.88	1.37	0.145	347	28818	403	24814	4005
ether	4.27	1.35	0.165	350	28571	408	24510	4062
THF	7.52	1.40	0.209	345	28986	405	24691	4294
dichloromethane	9.08	1.42	0.218	343	29155	404	24752	4402
DMF	36.7	1.43	0.276	342	29240	411	24331	4909
Acetone	21.01	1.36	0.285	341	29326	411	24331	4995
acetonitrile	37.5	1.34	0.305	339	29499	410	24390	5108

Table S5: Computed integral of hole and electron overlap (S), distance between centroids of hole and electron (D, Å) and dipole moment (μ) for singlet and triplet states of NSPI-DVP.

State	$\int h^+$	$\int e^-$	$\int T$	(S)	Centroid of hole (Å)			Centroid of electron (Å)			D (Å)	μ (a.u)
					x	y	z	x	y	z		
S1	0.8957	0.7208	0.0031	0.4276	0.5953	-1.2361	-0.0185	0.5880	-1.9110	-0.0162	0.67	1.03
S2	0.8896	0.7146	-0.0464	0.4042	-0.6101	-1.1399	0.0516	-0.4547	-1.7896	-0.0801	0.68	1.03
S3	0.7524	0.5916	0.0152	0.2608	0.5691	-0.3698	0.1723	-0.5292	0.9416	0.1885	1.71	2.17
S4	0.7444	0.5684	-0.0036	0.4379	-0.8255	-0.9119	0.1553	-0.0320	-0.8082	0.1584	0.80	0.99
S5	0.8286	0.6334	-0.0124	0.5190	2.8149	1.9270	0.1124	2.8846	2.2034	0.2634	0.32	0.44
T1	0.5629	0.4584	0.0181	0.2845	4.9144	-1.4134	0.1609	4.0253	-1.9221	0.1440	1.02	0.98
T2	0.5932	0.4801	-0.0433	0.2895	-4.779	-1.1907	-0.2592	-4.0851	-1.7185	-0.2339	0.87	0.88
T3	0.7933	0.5828	-0.0074	0.5112	2.8838	1.9932	0.1575	3.0570	2.2132	0.2741	0.30	0.39
T4	0.5702	0.4317	0.0097	0.3180	-0.1010	1.6974	-0.0266	-0.8192	1.6903	0.0344	0.72	0.68
T5	0.4799	0.3491	-0.0032	0.2897	-0.7116	1.2436	-0.0651	-0.4038	0.9019	0.0263	0.46	0.36

Table S6: Computed integral of hole and electron overlap (S), distance between centroids of hole and electron (D, Å) and dipole moment (μ) for singlet and triplet states of CNSPI-DVP.

State	$\int h^+$	$\int e^-$	$\int T$	(S)	Centroid of hole (Å)			Centroid of electron (Å)			D (Å)	μ (a.u)
					x	y	z	x	y	z		
S1	0.8359	0.6703	0.0033	0.4545	7.0447	-1.0825	-0.4466	7.2240	-1.5869	-0.0377	0.67	0.95
S2	0.8308	0.6591	-0.0002	0.4821	-7.3923	-1.4732	-0.0240	-8.0051	-1.5681	-0.1256	0.62	0.88
S3	0.8010	0.6237	-0.0065	0.3949	4.2179	0.6174	-0.3187	3.5344	1.5657	-0.0150	1.20	1.62
S4	0.7259	0.5676	0.0106	0.2474	-0.3211	-0.7816	0.2149	-0.7096	1.5870	0.1908	2.40	2.93
S5	0.7481	0.5663	-0.0090	0.4397	-0.0039	-1.2828	0.1805	-0.4602	-0.9678	0.1716	0.55	0.68
T1	0.5435	0.4283	0.0011	0.2957	6.7804	-1.1935	-0.3938	8.1560	-1.6922	-0.0215	1.50	1.38
T2	0.5289	0.4141	0.0019	0.3105	-7.0276	-1.4572	-0.0606	-8.6006	-1.4949	-0.0826	1.57	1.40
T3	0.6567	0.5028	-0.0068	0.3907	3.1023	1.7479	0.1622	3.2476	2.2483	0.0810	0.52	0.57
T4	0.6466	0.4872	0.0108	0.3662	-0.8849	2.5374	-0.0062	-0.8766	2.3694	0.0991	0.19	0.21
T5	0.3893	0.2724	-0.0046	0.2117	5.5380	0.0403	-0.7015	5.0595	0.2328	-0.4181	0.58	0.36

Table S7: Computed RMSD of electron and hole, H index and t index for singlet and triplet states of NSPI-DVP.

State	RMSD (Electron)				RMSD (Hole)				H index				t index			
	x	y	z	total	x	y	z	total	x	y	z	Total	x	y	z	Total
S1	8.584	1.280	0.981	8.734	8.425	1.560	1.303	8.667	8.504	1.420	1.142	8.697	-8.497	-0.745	-1.140	8.605
S2	8.919	1.428	1.005	9.088	8.634	1.543	1.339	8.873	8.777	1.486	1.172	8.978	-8.621	-0.836	-1.040	8.724
S3	2.301	2.856	0.746	3.743	3.310	2.373	0.921	4.175	3.310	2.805	2.614	0.834	-1.707	-1.303	-0.817	2.298
S4	3.362	2.776	0.784	4.430	3.822	2.272	0.866	4.530	3.592	2.524	0.825	4.467	-2.799	-2.420	-0.822	3.790
S5	2.351	1.925	1.375	3.335	2.490	1.799	1.333	3.349	2.420	1.862	1.354	3.341	-2.351	-1.586	-1.203	3.080
T1	7.196	1.463	0.929	7.402	7.252	1.603	1.152	7.516	7.224	1.533	1.041	7.458	-6.335	-1.024	-1.024	6.498
T2	8.176	1.382	1.013	8.353	7.898	1.413	1.238	8.118	8.037	1.398	1.125	8.235	-7.343	-0.870	-1.100	7.475
T3	2.379	1.858	1.381	3.320	2.306	1.871	1.323	3.251	2.343	1.864	1.352	3.285	-2.169	-1.644	-1.236	2.989
T4	3.302	3.546	0.835	4.917	3.514	3.783	0.932	5.247	3.408	3.664	0.883	5.082	-2.690	-3.657	-0.822	4.614
T5	3.344	3.800	0.867	5.135	3.681	4.025	0.906	5.529	3.513	3.913	0.886	5.332	-3.205	-3.571	-0.795	4.863

Table S8: Computed RMSD of electron and hole, H index and t index for singlet and triplet states of CNSPI-DVP.

State	RMSD (Electron)				RMSD (Hole)				H index				t index			
	x	y	z	total	x	y	z	total	x	y	z	Total	x	y	z	Total
S1	3.978	1.853	1.096	4.523	3.655	1.958	1.243	4.329	3.816	1.905	1.170	4.423	-3.637	-1.401	-0.761	3.971
S2	4.837	1.394	1.159	5.165	4.870	1.441	1.233	5.227	4.854	1.417	1.196	5.196	-4.241	-1.323	-1.095	4.575
S3	3.008	2.253	1.353	3.994	4.256	2.192	1.423	4.994	3.632	2.222	1.388	4.478	-2.948	-1.274	-1.084	3.390
S4	2.359	2.817	0.811	3.763	2.591	2.409	0.825	3.633	2.475	2.613	0.818	3.691	-2.086	-0.244	-0.794	2.246
S5	3.230	2.607	0.800	4.227	3.629	2.201	0.810	4.321	3.430	2.404	0.805	4.265	-2.973	-2.089	-0.796	3.720
T1	2.938	1.764	1.111	3.603	4.165	1.921	1.232	4.749	3.552	1.843	1.171	4.169	-2.176	-1.344	-0.799	2.680
T2	3.864	1.447	1.203	4.298	5.415	1.466	1.236	5.744	4.640	1.456	1.219	5.013	-3.067	-1.418	-1.197	3.585
T3	2.283	1.578	1.462	3.137	2.490	1.898	1.400	3.429	2.387	1.738	1.431	3.281	-2.241	-1.238	-1.350	2.894
T4	1.659	3.466	0.780	3.921	1.966	3.874	0.833	4.423	1.813	3.670	0.807	4.172	-1.804	-3.502	-0.701	4.001
T5	5.242	2.545	1.407	5.994	5.315	2.571	1.347	6.056	5.278	2.558	1.377	6.025	-4.800	-2.365	-1.093	6.025

Table S9. Transferred charges (q_{CT}), barycentres of electron density loss (R_+) /gain (R-), distance between two barycenters (D_{CT}), dipole moment of CT (μ_{CT}), RMSD of +ve/-ve parts, CT indices (H & t) and overlap integral of C+/C- of NSPI-DVP and CNSPI-DVP.

Blue emissive & Host materials	**q_{CT}** $\lvert e^{-1} \rvert$	**R_+ (Å)**			**R- (Å)**			**D_{CT} (Å)**	**μ_{CT} (D)**	**RMSD of +ve parts**	**RMSD of -ve parts**	**H / t indices (Å)**	**overlap integral of C+/ C-**
		x	y	z	x	y	z						
NSPI-DVP	0.000 -0.000	0.166	-0.588	-0.126	-0.319	-0.460	0.003	0.519	0.001	16.904	15.186	8.487/7.975	0.9928
CNSPI-DVP	22.076 -7.169	3.458	2.548	-0.837	-1.538	0.145	0.404	5.689	602.407	4.956	4.973	2.575/3.464	0.1778

Table S10. Summary of non- doped blue efficiencies with reported efficiencies.

Emitter	V_{on}(V)	L(cd/m^2)	EL(nm)	η_c(cd/A)	η_p(lm/W)	CIE(x,y)	ref
NSPI-DVP	**2.7**	**8932**	**439**	**5.61**	**4.99**	**0.15, 0.17**	**This work**
CNSPI-DVP	**2.6**	**7623**	**427**	**5.03**	**4.72**	**0.14, 0.13**	**This work**
Cz-DPVI	3.4	13629	419	4.9	4.3	(0.15,0.08)	3
PPI	3.8	3307	412	0.71	0.40	(0.161,0.065)	4
mTPA-PPI	3.2	4065	404	0.84	0.48	(0.161,0.049)	4
L-BPPI(50nm)	8.5	70	440	0.01	-	(0.16,0.11)	5
L-BPPI(40nm)	6.5	295	440	0.13	-	(0.16,0.11)	5
L-BPPI(30nm)	5.0	420	440	0.40	-	(0.16,0.10)	5
L-BPPI(20nm)	4.5	391	440	0.68	-	(0.16,0.10)	5
Z-BPPI(50nm)	6.5	105	440	0.07	-	(0.17,0.12)	5
Z-BPPI(40nm)	5.0	502	440	0.34	-	(0.16,0.12)	5
Z-BPPI(30nm)	4.5	267	440	0.45	-	(0.16,0.12)	5
Z-BPPI(20nm)	5.0	100	440	0.31	-	(0.16,0.11)	5
MADN(BUBD)	7.8	-	440	2.1	-	(0.15,0.10)	6
CPPPI	-	3322	420	0.65	0.48	(0.165,0.050)	7
PPICPPPI	-	4329	428	1.53	0.86	(0.166,0.056)	7
PhBPI	2.8	-	450	1.87	1.85	-	8
bilayer-TPBI	3.2	-	468	2.03	1.00	(0.15,0.15)	9
TPA-BPI	2.8	-	448	1.83	1.58	(0.15,0.09)	10
DPVBi	7.5	-	457	0.03	-	(0.15, 0.13)	11
DPVICz	4.2	-	470	0.92	-	(0.15, 0.22)	11
DPVTCz	3.8	-	470	1.94	-	(0.14, 0.22)	11
3,6-DPVTCz	5.0	-	449	0.11	-	(0.15, 0.11)	11
PEDOt-PSS:3(100nm)	4.0	2800	460	0.61	0.14	(0.15,0.14)	12
PEDOt-PSS:3(50nm)	3	10600	407	1.68	1.10	(0.16,0.13)	12
PEDOt-PSS:4(40nm)	2.5	21200	392	1.90	1.55	(0.16,0.14)	12
BBTPI	2.7	-	-	5.48	4.77	0.15, 0.10	13
BiPI-1	2.8	-	-	4.62	4.55	0.15, 0.08	14
3-CzPOPPI	2.9	-	-	2.71	2.73	0.15, 0.06	15
TTP-TPI	3.1	-	-	2.10	1.88	0.16, 0.05	16
DPT-TPI	2.9	-	-	3.13	3.22	0.16, 0.07	16
PMSO	3.2	-	-	4.64	4.0	0.152, 0.077	17
PPI-2TPA	3.0	-	-	4.40	4.60	0.150, 0.063	18
PPI-2NPA	3.0	-	-	3.98	3.88	0.151, 0.066	18
TPIBNCz	3.2	-	-	3.29	2.80	0.157, 0.074	19
PPi-Pid + CBP	3.15	-	-	4.13	-	0.151, 0.076	20

References

[1] (a) M. J. Frisch, G. W. Trucks, H. B. Schlegel, G. E. Scuseria, M. A. Robb, J. R. Cheeseman, G. Scalmani, V. Barone, B. Mennucci, G. A. Petersson, H. Nakatsuji, M. Caricato, X. Li, H. P. Hratchian, A. F. Izmaylov, J. Bloino, G. Zheng, J. L. Sonnenberg, M. Hada, M. Ehara, K. Toyota, R. Fukuda, J. Hasegawa, M. Ishida, T. Nakajima, Y. Honda, O. Kitao, H. Nakai, T. Vreven, J. A. Montgomery, J. E. Peralta, F. Ogliaro, M. Bearpark, J. J. Heyd, E. Brothers, K. N. Kudin, V. N. Staroverov, R. Kobayashi, J. Normand, K. Raghavachari, A. Rendell, J. C. Burant, S. S. Iyengar, J. Tomasi, M. Cossi, N. Rega, J. M. Millam, M. Klene, J. E. Knox, J. B. Cross, V. Bakken, C. Adamo, J. Jaramillo, R. Gomperts, R. E. Stratmann, O. Yazyev, A. J. Austin, R. Cammi, C. Pomelli, J. W. Ochterski, R. L. Martin, K. Morokuma, V. G. Zakrzewski, G. A. Voth, P. Salvador, J. J. Dannenberg, S. Dapprich, A. D. Daniels, O. Farkas, J. B. Foresman, J. V. Ortiz, J. Cioslowski, D. J. Fox, *Gaussian, Inc., Wallingford CT (Revision A.**02**), Gaussian, Inc., Wallingford., CT*. 2009.

[2] J. Jayabharathi, R. Ramyaa, V. Thanikachalam, P. Jeeva and E. Sarojpurani,*RSC Adv*., 2019, **9**, 2948-2966.

[3] H. Liu, Q. Bai, L. Ya, H. Zhan, H. Xu, S. Zhang, W. Li, Y. Gao, J. Li, P. Lu, H. Wang, B. Yang and Y. Ma, *Chem. Sci.,* 2015, **6**, 3797-3804.

[4] Z. Wang, Y. Feng, H. Li, Z. Gao, X. Zhang, P. Lu, P. Chen, Y. Mab and S. Liu, *Phys. Chem. Chem. Phys.,* 2014, **16**, 10837-10843.

[5] Y. F. Chang, H. F. Meng, G. L. Fan, K. T. Wong, H. W. Zan, H. W. Lin, H. L. Huang and S. F. Horn, *Org. Electron.*, 2016, **29**, 99-106.

[6] X. L. Li, X. Ouyang, D. Chen, X. Cai, M. Liu, Z. Ge, Y. Cao and S. J. Su, *Nanotechnol.,* 2016, **27**, 124001-124011.

[7] Y. Zhang, T. Wai, N. F. Lua, Q. X. Tong, S. L. Lai, M. Y. Chan, H. L. Kwong and C. S. Lee, *Dyes Pigm.*, 2013, **98**, 190-194.

[8] G. Li, J. Zhao, D. Zhang, J. Zhu, Z. Shi, S. Tao, Feng Lu and Q. Tong, *New J. Chem.,* 2017, **41**, 5191-5197.

[9] S. Liu, F. He, H. Wang, H. Xu, C. Wang, F. Li and Y. Ma, *J. Mater. Chem.,* 2008, **18**, 4802-4807.

[10] S. Kim, B. Sanyoto, W. T. Park, S. Kim, S. Mandal, J. C. Lim, Y. Y. Noh and J. H. Kim, *Adv. Mater.*, 2016, **28**, 10149-10154.